LANGMUIR Article
Cite This: Langmuir 2018, 34, 8939−8951
pubs.acs.org/Langmuir

Structure Dependence of Pyridine and Benzene Derivatives on Interactions with Model Membranes

Benjamin J. Peters,[†] Cameron Van Cleave,[†] Allison A. Haase,[†] John Peter B. Hough,[†,‡] Keisha A. Giffen-Kent,[†] Gabriel M. Cardiff,[†,§] Audra G. Sostarecz,[#] Dean C. Crick,[∥,⊥] and Debbie C. Crans*[,†,⊥]

[†]Department of Chemistry, [‡]Department of Biochemistry, [§]Department of Biology, [∥]Department of Microbiology, Immunology, and Pathology, and [⊥]Cell and Molecular Biology Program, Colorado State University, Fort Collins, Colorado 80523, United States
[#]Department of Chemistry, Monmouth College, Monmouth, Illinois 61462, United States

Supporting Information

ABSTRACT: Pyridine-based small-molecule drugs, vitamins, and cofactors are vital for many cellular processes, but little is known about their interactions with membrane interfaces. These specific membrane interactions of these small molecules or ions can assist in diffusion across membranes or reach a membrane-bound target. This study explores how minor differences in small molecules (isoniazid, benzhydrazide, isonicotinamide, nicotinamide, picolinamide, and benzamide) can affect their interactions with model membranes. Langmuir monolayer studies of dipalmitoylphosphatidylcholine (DPPC) or dipalmitoylphosphatidylethanolamine (DPPE), in the presence of the molecules listed, show that isoniazid and isonicotinamide affect the DPPE monolayer at lower concentrations than the DPPC monolayer, demonstrating a preference for one phospholipid over the other. The Langmuir monolayer studies also suggest that nitrogen content and stereochemistry of the small molecule can affect the phospholipid monolayers differently. To determine the molecular interactions of the simple N-containing aromatic pyridines with a membrane-like interface, ^{1}H one-dimensional NMR and ^{1}H−^{1}H two-dimensional NMR techniques were utilized to obtain information about the position and orientation of the molecules of interest within aerosol-OT (AOT) reverse micelles. These studies show that all six of the molecules reside near the AOT sulfonate headgroups and ester linkages in similar positions, but nicotinamide and picolinamide tilt at the water−AOT interface to varying degrees. Combined, these studies demonstrate that small structural changes of small N-containing molecules can affect their specific interactions with membrane-like interfaces and specificity toward different membrane components.

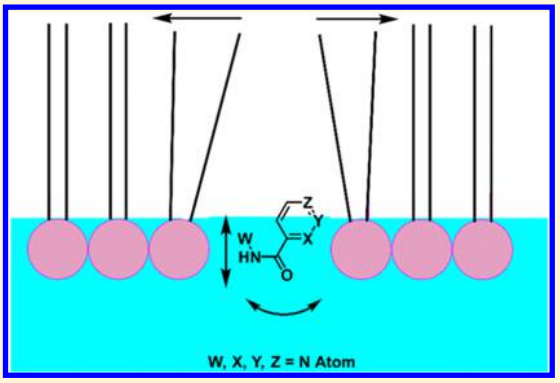

INTRODUCTION

Small molecules (<500 Da) have been the cornerstone for medical treatment, supplements, and preservatives, with many diffusing through the cellular membrane to reach their target.[1−5] One such example is a very successful first-line anti-tuberculosis drug, isoniazid (INH, Figure 1), which has been shown to diffuse across the membrane of *Mycobacterium tuberculosis*, where INH is then able to reach the target, KatG.[6,7] Similar to INH, the method of entry into a cell for many small molecules has been studied in detail,[8−12] but there is a lack of information pertaining to the specific interactions of small molecules with the membrane interfaces. This lack of information is in large part due to the difficulty of determining the specific interactions of molecules with the lipids that make up the membranes and the complexity of the biological membranes themselves.[13−15] The specific small-molecule−lipid interactions of a series of aromatic N-containing compounds were studied here (Figure 1) to understand how small molecules are taken into cells and how they affect the membrane and may elucidate aspects of the small molecules' mode of action.

Many of these small molecules, used to treat diseases such as tuberculosis, contain a pyridine as their main structural component.[16−18] The presence and placement of nitrogen within the pyridine ring have great affect on these small molecules and their inter- and intramolecular interactions. For example, the amide group of picolinamide (PIC) is ortho to the pyridine nitrogen, allowing for intramolecular hydrogen bonding (Figure 1).[19,20] This increases the molecule's hydrophobicity and allows it to penetrate a membrane interface deep enough to affect the packing of the phospholipid tails.[21,22] This behavior is not observed for nicotinamide (NIC, meta) nor isonicotinamide (iNIC, para) because the amide and pyridine nitrogens are not in proximity for intramolecular

Received: May 18, 2018
Revised: June 22, 2018
Published: June 29, 2018

DOI: 10.1021/acs.langmuir.8b01661
Langmuir 2018, 34, 8939−8951

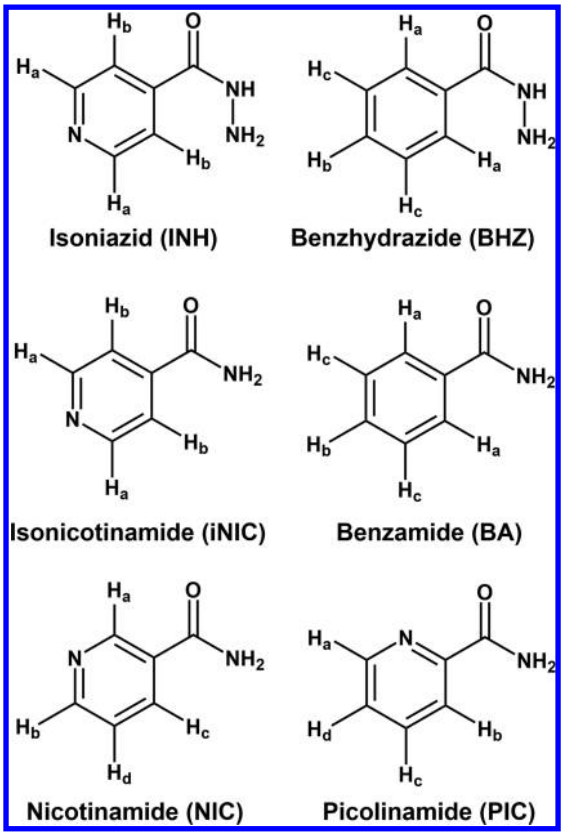

Figure 1. Structures of isoniazid (INH), benzhydrazide (BHZ), isonicotinamide (iNIC), benzamide (BA), nicotinamide (NIC), and picolinamide (PIC), with protons labeled for ^{1}H NMR peak labeling. The protons in the ^{1}H NMR spectra have H_a as the most downfield ^{1}H NMR peak, H_b as the next one, etc. See Figure S1 for enlarged versions.

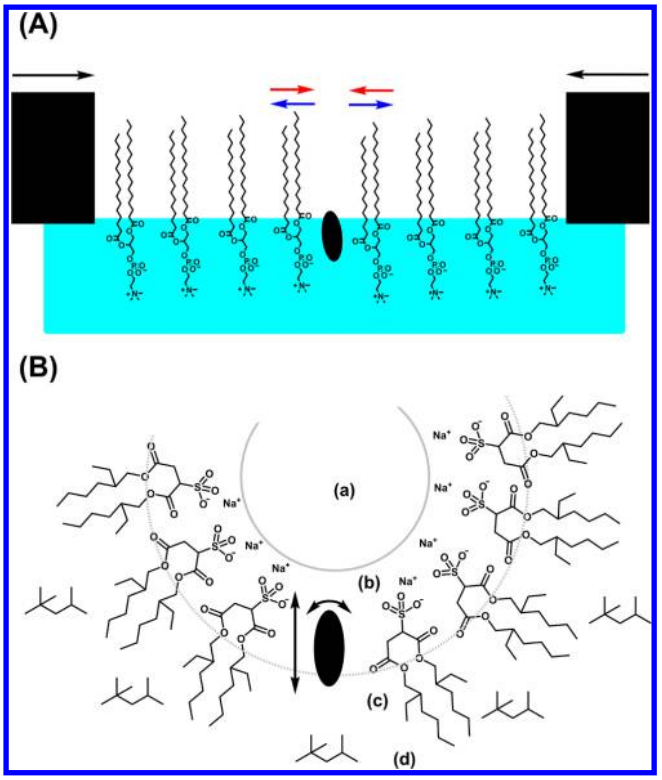

Figure 2. Langmuir monolayer (A) showing how a molecule can affect a phospholipid interface by penetrating and condensing (red arrows) or spreading (blue arrows) the phospholipids during a compression isotherm. The schematic depiction of a RM (B) outlining the area in which a molecule may reside, such as the bulk water (a), interfacial Stern layer (b), AOT tail region (c), and isooctane (d). The black oval demonstrates how a molecule can have varying depths within the RM interface along with different orientations. Figure adapted from Peters *et al.*[30]

hydrogen bond formation.[19,20] Despite this difference, Olsson *et al.* were able to show that NIC tightly binds to plasma membrane extracts of human leukemic K-562 cells (K_d between 3.2 and 12.7 μM).[9] Because such small differences in structure have such profound effects on inter- and intramolecular interactions, we hypothesize here that these molecules may interact with a membrane interface differently despite having similar structures, as shown in Figure 1.

To study how small structural differences can affect interactions with membrane interfaces, this study aims to explore the interactions of the molecules shown in Figure 1 with two model membrane interfaces (Figure 2). The first model membrane, Langmuir monolayer, has been used to obtain free energies of mixing of hydrophobic molecules,[23−25] explore phenomena within the membrane,[26−28] and to test how molecules affect a lipid interface.[29−32] While compressing a phospholipid Langmuir monolayer in the presence of the molecules shown in Figure 1, it is possible to determine if the molecules expand, reorganize, or affect the compressibility of the phospholipid monolayer.[33] A commonly used phospholipid, dipalmitoylphosphatidylcholine (DPPC), can comprise up to 40% of lung phospholipid content because of its superior ability to expand and spread at the lung alveolar air−liquid interface.[34−36] Similarly, dipalmitoylphosphatidylethanolamine (DPPE) is utilized to model the inner leaflet of bacterial and eukaryotic membranes for drug and lipid interactions.[37,38] These two lipids have become a very appealing model interface to study drug and lipid interactions and therefore were used in this study as a model membrane interface to study the interactions of the N-containing compounds in Figure 1.[34−38] To determine the molecular details of interactions of small aromatic N-containing compounds with an interface, their interactions with aerosol-OT (AOT) reverse micelles (RMs)[39−42] were examined.[30,43−47] RMs are self-assembled microemulsions that form at low water concentration. In these systems, the placement and orientation could be identified by monitoring interactions with the AOT headgroup and/or lipid tails using one-dimensional (1D) and two-dimensional (2D) NMR spectroscopic techniques.[30,43−47] With the combination of these two model membrane systems (Figure 2), information about how the compounds in Figure 1 interact with membrane-like interfaces was obtained in this study.

MATERIALS AND METHODS

General Materials. Most materials were used without further purification. Benzamide (BA) (99%), PIC (98%), NIC (98%), iNIC (99%), INH (≥99%), benzhydrazide (BHZ) (98%), isooctane (2,2,4-trimethylpentane, 99.8%), methanol (≥99.9%), activated charcoal (99.5%), chloroform (≥99.5%), deuterium oxide (99.9%), 2,2-dimethyl-2-silapentane-5-sulfonate sodium salt (DSS, 97%), monosodium phosphate (≥99.0%), disodium phosphate (≥99.0%), sodium hydroxide (≥98%), and hydrochloric acid (37%) were all purchased from Sigma-Aldrich. DPPC (≥99%) and DPPE (99%) were purchased from Avanti Polar Lipids. Sodium aerosol-OT (AOT) (bis(2-ethylhexyl)sulfosuccinate sodium salt, ≥99.0%) was purchased from Sigma-Aldrich and was purified further as has been reported

DOI: 10.1021/acs.langmuir.8b01661
Langmuir 2018, 34, 8939−8951

previously to remove any acidic impurities.[30] Briefly, 50.0 g of AOT was dissolved into 150 mL of methanol to which 15 g of activated charcoal was added. This suspension was stirred for 2 weeks. After mixing, the suspension was filtered to remove the activated charcoal. The filtrate was then dried under rotary evaporation at 50 °C until the water content was below 0.2 molecules of water per AOT as determined by ^{1}H NMR spectroscopy. The pH was adjusted throughout this study using varying concentrations of NaOH or HCl dissolved/mixed in either D_2O or H_2O depending on experimental requirements. NaOH or HCl dissolved in D_2O is referred to as NaOD or DCl, respectively.

Preparation of Phospholipid Langmuir Monolayers. Phospholipid stock solutions were prepared by dissolving DPPC (0.018 g, 0.025 mmol) or DPPE (0.017 g, 0.025 mmol) in 25 mL of 9:1 chloroform/methanol (v/v) for a final concentration of 1 mM phospholipid. The aqueous subphase consisted of 50 mL of 20 mM sodium phosphate buffer (pH 7.4) and varying concentrations of hydrazide of amide (10, 1.0, 0.10, or 0 mM hydrazide or amide). Sodium phosphate buffer (20 mM, pH 7.4) instead of distilled deionized H_2O (DDI H_2O) was used as the subphase for the compression isotherms for better pH control (Figure S2).[30] Before addition of the phospholipid monolayers, the surface of the subphase was cleaned using vacuum aspiration, and to make sure the surface was clean, the surface pressure of a compression isotherm of just the subphase (no phospholipid present) was measured (surface pressure was consistently 0.0 ± 0.5 mN/m throughout compression). To prepare the phospholipid monolayer, 20 μL of phospholipid stock solution (20 nmol of phospholipid, 112 Å^2/molecule) was added to the surface of the subphase in a dropwise manner using a Hamilton syringe. The film was allowed to equilibrate for 15 min. The resulting phospholipid monolayer was then used for the compression isotherm experiments (see Figure 2A).

Compression Isotherm Surface Pressure Measurements of Langmuir Monolayers. The phospholipid monolayer was compressed from two sides with a total speed of 10 mm/min (5 mm/min from opposite sides, Figure 2A) using Kibron μTroughXS equipped with a Teflon ribbon (poly(tetrafluoroethylene), hydrophobic barrier). The temperature was maintained at 25 °C using an external water bath.

The surface tension of the subphase during each compression was monitored using a wire probe as a Wilhemy plate. The surface pressure was calculated from the surface tension using eq 1, where π is the surface pressure, γ_o is the surface tension of water (72.8 mN/m), and γ is the surface tension at a given area per phospholipid after the film has been applied.

$$\pi = \gamma_o - \gamma \quad (1)$$

Each compression isotherm experiment consisted of at least three replicates, and the averages with standard deviations of the area per phospholipid at every 5 mN/m were calculated using Microsoft Excel. The worked-up data were transferred to OriginPro version 9.1 to be graphed. From the averages of the compression isotherms, the percent differences from the control of each sample at 5, 30, and 35 mN/m were calculated. The compression moduli were calculated using OriginPro version 9.1 from the compression isotherm average results using eq 2, where C_s^{-1} is the compression modulus, A is the surface area, and π is the surface pressure.

$$C_s^{-1} = -A(d\pi/dA) \quad (2)$$

Preparation of RMs for Dynamic Light Scattering (DLS). RMs were prepared as has previously been reported.[30] To prepare the 100 mM AOT stock solution, 2.2 g of purified AOT (4.9 mmol) was dissolved into 50 mL of isooctane. The 10 mM aqueous stock solutions of amide or hydrazide were prepared by dissolving 50 μmol of amide or hydrazide into 5 mL of DDI H_2O, and then the pH was adjusted to pH 7.0. To prepare the RM solutions, specific volumes of the AOT stock solution and aqueous solution were added for a total of 5 mL to form RM sizes of w_0 8, 12, 16, and 20, where $w_0 = [H_2O]/[AOT]$. Upon mixing the AOT stock solution with aqueous solution, a white aggregate formed at the water−isooctane interface. Then, the mixture was vortexed until clear (∼30 s), consistent with the formation of RMs.[30]

Parameters for DLS Analysis. Once the glass cuvettes (1 cm × 1 cm) had been washed with isooctane and RM sample (three times each), the cuvettes were filled with 1 mL of sample and analyzed using Zetasizer Nano ZS. The wavelength of light used was 632.8 nm, and scattering was obtained at an angle of 173°. Each sample was equilibrated for 700 s at 25 °C and then run for 10 scans per acquisition for 15 acquisitions. Each sample was run in triplicate, and the hydrodynamic radii (R_h) and polydispersity index were averaged with the standard deviations reported in Table S1.

Preparation of Aqueous Stock Solutions of Amides and Hydrazides for RM Samples for ^{1}H NMR. The aqueous stock solutions were prepared by dissolving 0.25 mmol (0.50 mmol for NIC) of amide or hydrazide into 25 mL of D_2O for a final concentration of 10 mM (20 mM for NIC). The NIC concentration was increased to obtain a greater signal-to-noise ratio in the ^{1}H NMR spectra of the RMs. Each aqueous stock solution was then pipetted into 2 mL aliquots, and the pD (pD = pH + 0.4)[30,46] of each aliquot was adjusted using NaOD or DCl solutions (5.0, 1.0, and 0.1 M). The pD will be referred to as pH in the rest of this article as is commonly done.[30,46] The pD of the aliquots was adjusted to a range between 1.2 and 9.0 for later use in the determination of the pK_a in D_2O and in the w_0 16 RMs.

Preparation of AOT−Isooctane Stock Solution and RMs for ^{1}H NMR. The 750 mM AOT stock solution was prepared by dissolving 8.34 g of AOT (18.8 mmol) in 25 mL of isooctane. This mixture was sonicated and vortexed until clear (approximately 15 min). Once dissolved, the solution was equilibrated to ambient room temperature. RMs of w_0 values of 8, 12, 16, and 20 were prepared by adding specific volumes of the stock AOT solution and the pH 7.0 aqueous aliquot. The other aqueous aliquots (215 μL) of pH's ranging from 1.2 to 9.0 and the AOT stock solution (785 μL) were mixed to form w_0 16 RMs at varying pH values. The indicated pH values of the RMs are assumed to be the same from the measured aqueous samples. All of the RM mixtures were vortexed until clear as was done for DLS experiments.

^{1}H NMR of D_2O and RM Samples. The ^{1}H NMR experiments were performed using a 400 MHz Varian NMR spectrometer using standard parameters (1 s relaxation time, 25 °C, and 45° pulse angle). The aqueous samples were referenced to an external DSS sample at pH values of 1.2, 1.5, 2.0, 2.5, and 3.0. Above pH 3.0, the DSS methyl silane peak was consistent and therefore the pH 3 DSS standard was used as the standard for the aqueous samples at higher pH values. RM samples were referenced to the isooctane methyl peak at 0.90 ppm as has been previously reported and were originally referenced to tetramethylsilane.[30,43,46] The resulting spectra were analyzed using MestReNova version 10.0.1. The pK_a values were determined by plotting the chemical shifts of the samples at different pH values in D_2O and in w_0 16 RMs and then taking the first derivative of the best-fit curve using OriginPro version 9.1 (see Figure S3).[30]

Preparation of RMs for ^{1}H−^{1}H 2D Nuclear Overhauser Enhancement Spectroscopy (NOESY) and Rotating-Frame Overhauser Effect Spectroscopy (ROESY) NMR. The 750 mM AOT stock solution was prepared by dissolving 0.34 g of AOT (0.76 mmol) in 1 mL of isooctane. To form the RM (w_0 12), 839 μL of the AOT stock solution was added to 161 μL of D_2O and vortexed until clear. This suspension was then mixed with 32 μmol of amide or hydrazide for an average concentration of 200 mM amide or hydrazide within the RM water pool (32.2 mM overall). The mixture was vortexed until the solid dissolved into the RM microemulsion.

Parameters for Recording the ^{1}H−^{1}H 2D NOESY and ROESY NMR Spectra. The ^{1}H−^{1}H 2D NOESY and ROESY experiments were conducted using 400 MHz Varian NMR at 26 °C with 16 scans per transient and 256 transient pairs in the f1 dimension. The ^{1}H−^{1}H 2D NOESY spectrum was acquired using a standard pulse sequence with a mixing time of 200 ms and a 1.5 s relaxation delay. The ^{1}H−^{1}H 2D ROESY spectra were acquired using a standard pulse sequence with a 200, 100, or 0 ms mixing time and a 1.5 s relaxation delay. The resulting spectra were analyzed using MestReNova version 10.0.1 by

DOI: 10.1021/acs.langmuir.8b01661
Langmuir 2018, 34, 8939−8951

subjecting the spectra to a 90° sine^2 weighting function with a first point at 0.50. The spectra were then phased and baselined using a third-order Bernstein polynomial baseline. Each spectrum was referenced to the isooctane methyl peak at 0.904 ppm in both dimensions.[30]

RESULTS AND DISCUSSION

Interactions of Aromatic Hydrazides with Langmuir Monolayers. Surface pressure compression isotherms of DPPC and DPPE were measured to model phospholipids commonly found in eukaryotic and bacterial membranes.[34−38] The minor structural difference in the lipid headgroup results in significant differences in the properties of the resulting lipid monolayer. DPPE has a conical shape and packs much more tightly when compared with DPPC, which has a cylindrical shape. This is thought to be due to the hydrogen bonding capability of DPPE (ethanolamine headgroup) that DPPC (choline headgroup) is lacking.[48,49] For these reasons, both DPPC and DPPE zwitterionic phospholipids were used to form Langmuir monolayers to study the interactions of small molecules with phospholipid interfaces.

Surface pressure compression isotherms of DPPC or DPPE were initially conducted in the presence of INH or BHZ hydrazides (Figure 3A−D). The area per phospholipid of the

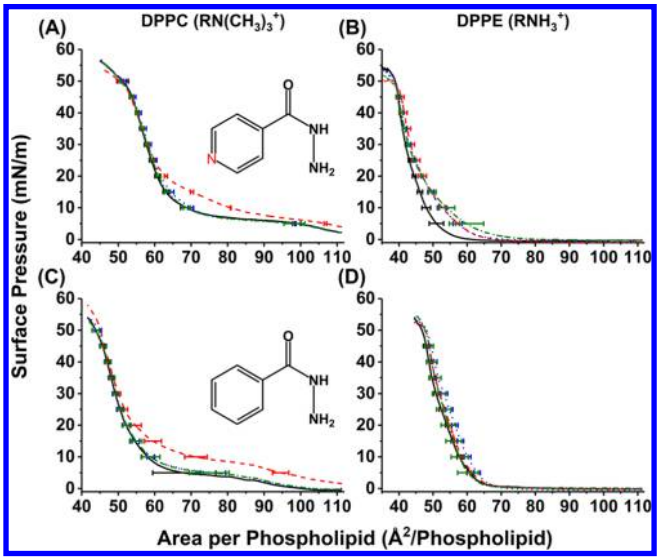

Figure 3. Average compression isotherm curves of DPPC (left column) or DPPE (right column) in the presence of INH (A, B) or BHZ (C, D). The solid black curves correspond to the control films without any hydrazide present. The other curves correspond to 10 mM (red dashed line), 1 mM (blue dotted line), and 0.1 mM (green dashed and dotted line) hydrazide present in the 20 mM sodium phosphate buffered subphase (pH 7.4). Each curve is an average of at least three trials with standard deviations. The R group for each phospholipid includes the phosphate, glycerol, and fully saturated C_{16} tails. See Figures S4 and S5 for enlarged versions.

DPPC monolayer in the presence of 10 mM INH increased, until 20−25 mN/m. The area per phospholipid of the DPPE monolayer in the presence of all concentrations of INH tested increased until 25−30 mN/m. In the presence of 10 mM BHZ, the area per phospholipid of the DPPC monolayer increased until 15−20 mN/m and the area per phospholipid of the DPPE monolayer was unaffected. Briefly, INH affected the area per phospholipid of both monolayers, but all concentrations affected the DPPE monolayer. BHZ affected only the area per phospholipid of the DPPC monolayer.

To determine if the compressibility of the monolayers was affected, the compression modulus was calculated from the average compression isotherms (Figure S6). In the presence of 10 mM INH, the compression modulus of the DPPC monolayer decreased and all concentrations of INH tested caused a decrease in the compression modulus of the DPPE monolayer. The presence of 10 mM BHZ decreased the compression modulus of the DPPC monolayer and increased the compression modulus in the presence of 1 mM BHZ. All concentrations of BHZ tested increased the compression modulus of the DPPE monolayer. In summary, INH decreased the compression modulus of both DPPC and DPPE monolayers, but only the DPPE monolayer was affected at all concentrations tested. BHZ decreased the compression modulus of the DPPC monolayer, and with 1 mM BHZ present, the compression modulus of the DPPE monolayer increased.

Generally, an increase in area per phospholipid of a monolayer indicates an uptake of the small molecule, causing the monolayer to spread, and a decrease in area per phospholipid indicates either solubilization of lipid or a reorganization to allow for tighter packing of the phospholipid monolayer. A decrease in compression modulus has been commonly interpreted as an increase in compressibility and vice versa.[29,50] INH did increase the area per phospholipid of both the DPPC and DPPE monolayers, indicating an uptake into the phospholipid monolayers, but did so at lower concentrations present for DPPE. A similar trend was observed with the decrease of compression moduli in the presence of INH. This suggests that INH has a higher affinity for DPPE than DPPC, indicating that INH would interact more favorably with the ethanolamine than with the choline headgroup. This is presumably due to hydrogen bonding with the ethanolamine headgroup, which would disrupt the intermolecular hydrogen bonding between individual DPPE molecules of the DPPE monolayer.[48,49] BHZ affected the area per phospholipid of only the DPPC monolayer at 10 mM and decreased the compression modulus, suggesting that at high concentration, BHZ is taken inside and allows for easier compression of the DPPC monolayer. At 1 mM for DPPC and all concentrations tested for DPPE, BHZ does not affect the area per phospholipid but increases the compression modulus, showing that the BHZ did not spread the phospholipids but did cause the monolayer to be more difficult to compress than the control monolayers. This suggests that BHZ is reorganizing the phospholipid tails, but more information would be needed for confirmation. In summary, INH was shown to prefer the ethanolamine headgroup and allowed for easier compression than the control phospholipid monolayers, whereas BHZ allowed for easier compression and spread the DPPC monolayer when 10 mM was present in the subphase but, otherwise, caused the phospholipid monolayers to be less compressible without affecting the area per phospholipid.

Interactions of Aromatic Amides with Langmuir Monolayers. To determine if the amides in Figure 1 interact with phospholipid interfaces differently, the surface pressure compression isotherms of DPPC and DPPE were conducted in the presence of BA, PIC, NIC, and iNIC, shown in Figure 4, and compression moduli are given in Figure S11.

First, the compression isotherm experiments using BA were conducted as a nitrogen-deficient comparison. In the presence

DOI: 10.1021/acs.langmuir.8b01661
Langmuir 2018, 34, 8939−8951

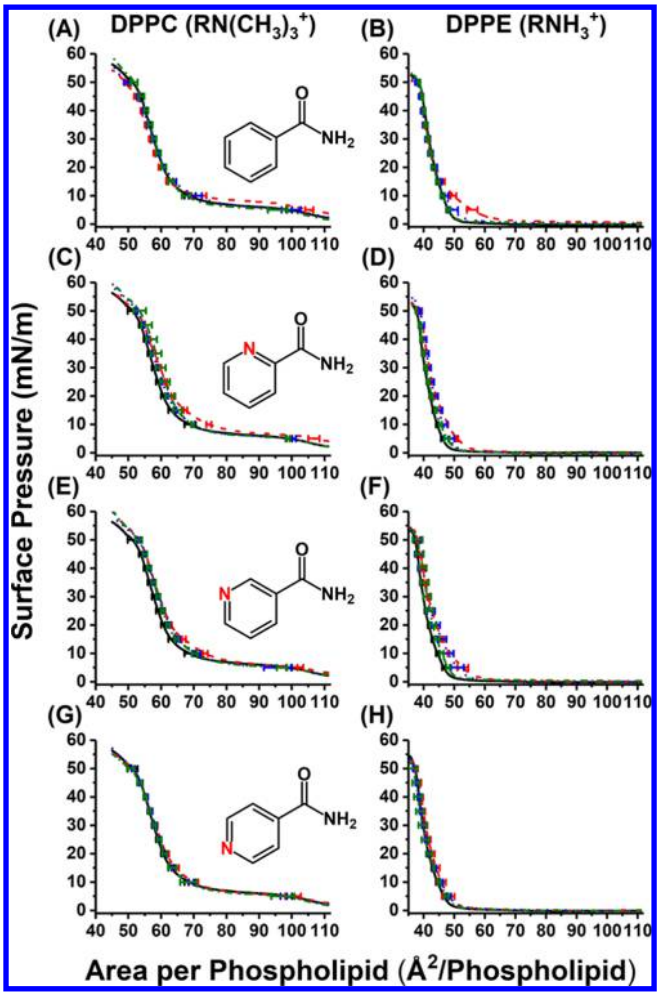

Figure 4. Resulting average surface pressure compression isotherms of DPPC (left column) and DPPE (right column) in the presence of BA (A, B), PIC, (C, D), NIC (E, F), and iNIC (G, H) at concentrations of 0 mM (black solid line), 0.1 mM (green dashed and dotted line), 1.0 mM (blue dotted line), and 10 mM (red dashed line) in the 20 mM sodium phosphate buffered subphase (pH 7.4). Each curve is an average of at least three trials with standard deviations. The R group for each phospholipid includes the phosphate, glycerol, and fully saturated C_{16} tails. See Figures S7–S10 for enlarged images.

of 10 mM BA, the DPPC monolayer exhibited an increase in pressure below 15–20 mN/m and then above 15–20 mN/m exhibited a slight decrease in area per phospholipid. The DPPE monolayer increased in area per phospholipid until 15–20 mN/m. The compression modulus (Figure S11) of the DPPC monolayer decreased in the presence of 10 and 0.1 mM BA and increased when 1.0 mM was present. Concentrations of 10 and 0.1 mM BA also decreased the compression modulus of the DPPE monolayer. This data suggests that BA can spread the phospholipids of both DPPC and DPPE until higher pressures, but it can still affect the compressibility of the phospholipid monolayers, showing that BA still does interact with the monolayer at higher pressures.

In the presence of 10 mM PIC, the DPPC and DPPE monolayers exhibited an increase in area per phospholipid as compared with the control monolayers until 35–40 mN/m. Also, depending on the concentration of PIC within the subphase, the compression modulus for DPPC decreased (10 mM), increased (1 mM), or no effect was observed (0.1 mM). The DPPE monolayer compression modulus was increased only by the presence of 0.10 mM PIC. The increase in area per phospholipid of DPPC and DPPE in the presence of PIC suggests that PIC is spreading the lipids, but depending on the concentrations of PIC, the compressibility of the phospholipid monolayers is affected (Figure S11). The dependence of the compressibility on the concentration may be due to counteracting effects where a large amount of PIC (10 mM) increases compressibility solely because PIC exists in excess within the monolayer, so it is compressed out of the monolayer. At lower concentrations (1 mM for DPPC and 0.10 mM for DPPE), PIC caused the monolayers to become more rigid and less compressible. Briefly, PIC did increase the area per phospholipid of both phospholipid monolayers and had varying effects on the compression moduli of the phospholipid monolayers.

The DPPC and DPPE monolayers in the presence of NIC both exhibited an increase in area per phospholipid. All concentrations of NIC tested increased the area per phospholipid of DPPC above 10 mN/m. The DPPE monolayer was affected in a concentration-dependent manner where 10 mM NIC increased the area per molecule the most. The presence of 10 mM NIC caused an increase in area per phospholipid of DPPE across at all surface pressures below collapse (55 mN/m). There was not much of an effect of NIC on the compression modulus of the DPPC monolayer (Figure S11); however, there was a decrease in the compression modulus for the DPPE monolayer at all concentrations of NIC tested. The presence of NIC caused a spreading of both phospholipid monolayers but only affected the compressibility of the DPPE monolayer, allowing it to become more compressible than the control monolayer.

Unlike the other molecules tested, iNIC had no effect on either the DPPC or the DPPE monolayer area per phospholipid. The presence of 10 and 1.0 mM iNIC did however decrease the compression modulus of the DPPE monolayer but did not have much of an effect on the compressibility of the DPPC monolayer (Figure S11). This suggests that iNIC has a higher affinity for DPPE than for DPPC and allows the DPPE monolayer to be more easily compressed without spreading the phospholipids.

By comparing the interactions of all of the molecules of interest with DPPC and DPPE monolayers, it is clear that not all of the aromatic N-substituted compounds interact with the phospholipid monolayers in the same manner (Figure 4 and Table 1). Out of the six compounds tested, INH and iNIC exhibited more of an effect on the DPPE monolayer than on the DPPC monolayer, suggesting a preference for the ethanolamine headgroup more so than for the choline headgroup. This is most likely due to the ethanolamine's greater hydrogen bonding capacity than that of choline, allowing for intermolecular interaction. When comparing PIC, NIC, and iNIC, the data is consistent with PIC and NIC, affecting the phospholipid monolayers similarly, but iNIC had the least effect on the phospholipid monolayers. As shown in Table 1, NIC and PIC were the only compounds to significantly increase the area per phospholipid of the DPPC and DPPE monolayers at physiologically relevant surface pressures (30–35 mN/m),[51] whereas iNIC did not have much of an effect on the area per phospholipid. Of all of the compounds, BA was the only molecule to cause a decrease in area per phospholipid for DPPC at higher surface pressures (above 15–20 mN/m, Table 1), suggesting that BA was the only compound tested that either reorganized DPPC to

DOI: 10.1021/acs.langmuir.8b01661
Langmuir 2018, 34, 8939–8951

Table 1. Percent Difference of Monolayer Surface Area in the Presence of Aromatic N-Substituted Compounds[a]

		DPPC	DPPE
compound	surface pressure (mN/m)	% difference from control	% difference from control
INH	5	7.36	12.25
	30	0.89	3.61
	35	0.10	3.22
BHZ	5	38.84	1.06
	30	1.86	2.02
	35	1.14	1.95
BA	5	6.21	16.19
	30	−2.20*	−0.92
	35	−2.19*	1.46
PIC	5	2.41	7.65
	30	3.32*	3.65**
	35	2.47**	3.44**
NIC	5	3.42	13.33
	30	3.01**	4.08**
	35	2.77**	3.62**
iNIC	5	1.22	3.32
	30	1.03	1.87
	35	0.55	1.89

[a]Surface pressures were chosen based on initial curve (5 mN/m) and physiological relevance (30−35 mN/m).[51] Significance of the percent difference was determined using Student's t test with *$p < 0.10$ and **$p < 0.05$.

condense further or assist in the solvation of the DPPC. Interestingly, BHZ did not have the same effect as BA but still interacted with the phospholipid monolayers, causing the phospholipids to spread. In summary, INH and iNIC both exhibited a preference for DPPE over DPPC, PIC and NIC affect the phospholipid monolayers similarly even at high pressures, BA reorganizes the DPPC monolayer or helps solubilize the DPPC, and BHZ does interact with both monolayers, causing spreading of the phospholipids.

Placement of Small Aromatic Hydrazides and Amides within the AOT RM. Molecular information on the specific interaction and placement of the compounds with respect to a membrane interface was sought using AOT RMs and NMR spectroscopy.[30,43−47,52] To this end, the ^{1}H NMR spectrum of each N-containing compound was acquired in D_2O and varying sizes of RM. By varying the sizes of the RM (w_0), small changes in the RM microenvironment occur. Comparing the chemical shifts of the N-containing compounds caused by varying environmental differences, it is possible to place the compounds within the RM.[30,43−47,52] The following paragraphs describe the chemical shifting and our placement of compounds as a result of the observed chemical shifting patterns.

The ^{1}H NMR spectra of INH and iNIC are presented as stack plots of ^{1}H NMR spectra in D_2O at the bottom and the RM microemulsions with the smallest RMs as the top spectrum (w_0 8, Figure 5). In the INH spectra, the H_a doublet peak shifts slightly downfield from the D_2O spectrum at 8.67−8.71 ppm in the w_0 20 spectrum and then gradually shifts upfield to 8.70 ppm in the w_0 8 spectrum. The doublet H_b peak for INH shifted gradually downfield from 7.69 ppm in D_2O to 7.80 ppm in the w_0 8 spectrum. A similar shifting pattern was observed with iNIC. The peak corresponding to the doublet H_a for iNIC barely shifts from 8.70 ppm in D_2O to 8.74 ppm in the w_0 20 spectrum followed by a slight upfield shift to the w_0 8 spectrum at 8.72 ppm. The doublet peak corresponding to H_b shifts gradually downfield from 7.76 ppm in the D_2O spectrum to 7.86 ppm in the w_0 8 spectrum. The downfield shifting of both H_a and H_b peaks of INH and iNIC from the D_2O spectrum to the w_0 20 spectrum is consistent with a more charged (deshielded) environment interpreted as placement near the sulfonates of the AOT.[53] The upfield shifting pattern of H_a of both compounds is consistent with the reduction of a charged environment as the RM sizes are reduced, suggesting that H_a is more toward the hydrophobic region than H_b.[53] Together this data suggests that both INH and iNIC reside near the AOT headgroups with the pyridine nitrogen facing toward the AOT tails and the amide/hydrazide toward the water pool similar to benzoate and phenyl biguanide.[30,46]

Next, the interactions of the benzene-based hydrazide and amide, BHZ and BA, with the AOT RM interface are described by ^{1}H NMR. The doublet corresponding to H_a for BHZ shifted from 7.74 ppm in the D_2O spectrum to 7.94 ppm gradually as the RM sizes were reduced to the w_0 8 spectrum.

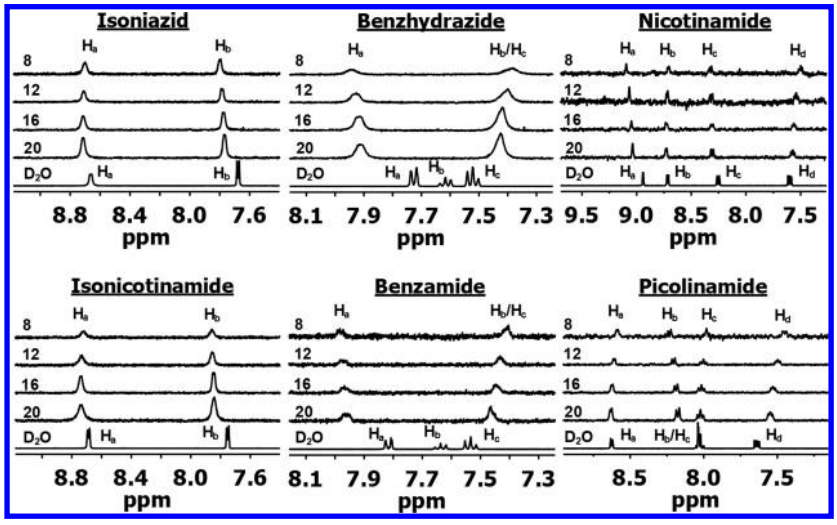

Figure 5. One-dimensional (1D) ^{1}H NMR spectra obtained using a 400 MHz Varian NMR of INH, iNIC, BHZ, BA, NIC, and PIC in D_2O and varying sizes of RMs (w_0) given on the left of each stack of spectra. See Figure 1 for labeled structures corresponding to peak labels.

DOI: 10.1021/acs.langmuir.8b01661
Langmuir 2018, 34, 8939−8951

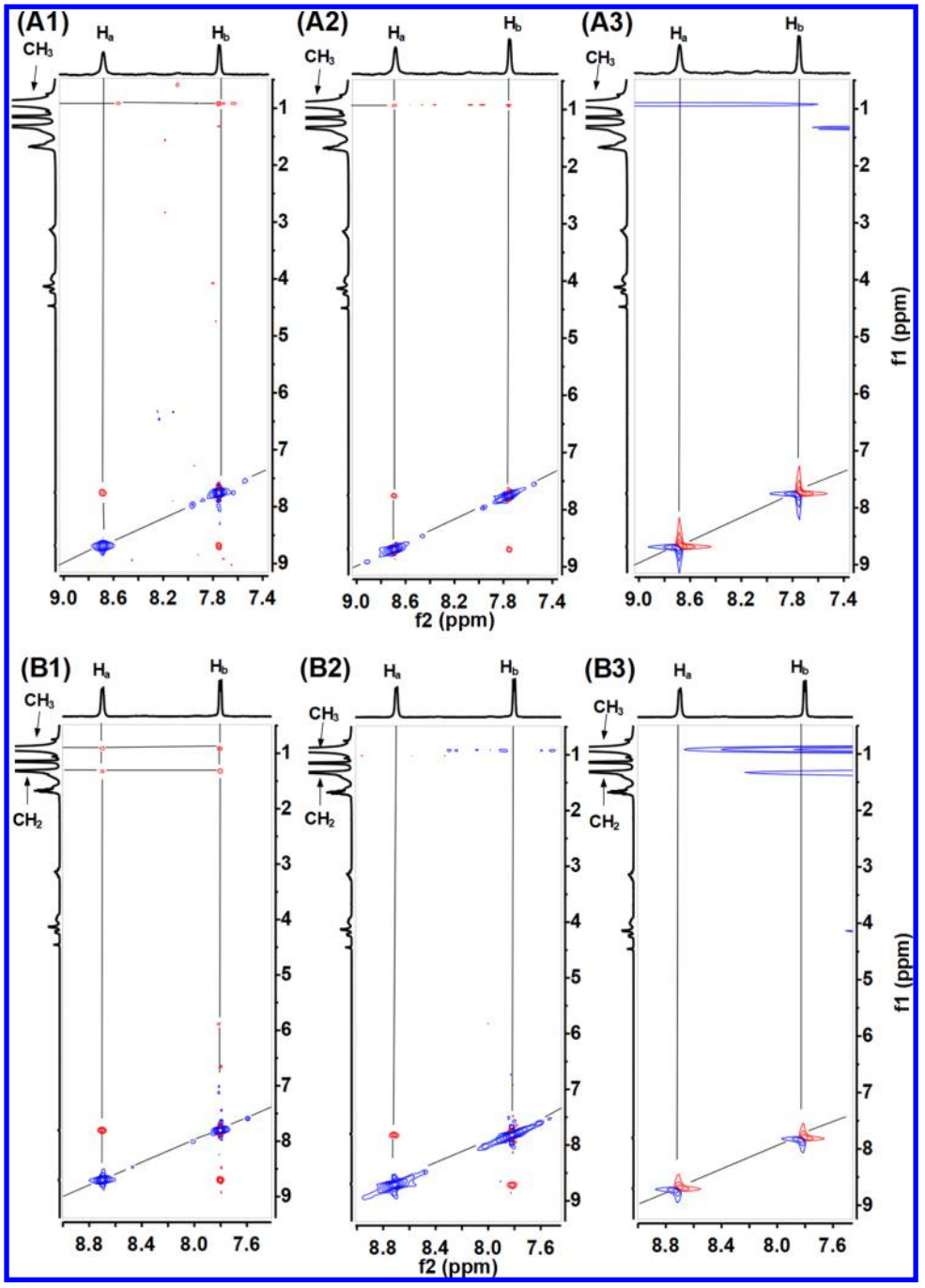

Figure 6. $^{1}H-^{1}H$ 2D ROESY NMR spectra acquired using a 400 MHz Inova NMR of INH (A1−A3) and iNIC (B1−B3) using 200, 100, and 0 ms mixing times (1−3) and a relaxation delay of 1.5 s. The diagonal is indicated by the diagonal line. The lines also highlight any off-diagonal cross-peaks.

The triplets corresponding to H_b and H_c for BHZ are at 7.62 and 7.52 ppm, respectively, in the D_2O spectrum and then coalesce in the RM spectra while gradually shifting upfield to 7.38 ppm in the w_0 8 spectrum. The peak corresponding to H_a for BA shifts from 7.83 ppm in D_2O gradually to 7.99 ppm in the w_0 8 spectrum. The peaks corresponding to H_b and H_c of BA in the D_2O spectrum are at 7.64 and 7.53 ppm, respectively, and then coalesce in the RM spectra and gradually shift upfield until 7.40 ppm in the w_0 8 spectrum. The downfield shifting pattern of H_a for both BHZ and BA from the D_2O spectrum to the w_0 8 spectrum is consistent with the RM interface. The upfield shifting pattern of H_b and H_c of both BHZ and BA is consistent with a deep placement within the RM interface toward the AOT tails. Using this data, it is possible to place BHZ and BA within the water−AOT interface with the benzene ring of both compounds placed a little more toward the AOT tails than INH and iNIC and with the amide/hydrazide toward the water pool. This is similar to what has been previously found for benzoic acid.[30]

The position and orientation of NIC within the RM were explored by itself unlike the previous compounds. The doublet corresponding to H_a for NIC shifted gradually downfield from 8.94 ppm in the D_2O spectrum to 9.10 ppm in the w_0 8 spectrum. The H_b doublet shifts from 8.72 ppm in the D_2O

DOI: 10.1021/acs.langmuir.8b01661
Langmuir 2018, 34, 8939−8951

spectrum to 8.74 ppm in the w_0 20 spectrum and then shifts upfield to 8.71 ppm in the w_0 8 spectrum. The H_c doublet shifts from 8.27 ppm in the D_2O spectrum gradually to 8.34 ppm in the w_0 8 spectrum, and the H_d peak is the only peak for NIC to gradually shift upfield from 7.62 ppm in the D_2O spectrum to 7.52 ppm in the w_0 8 spectrum. The downfield shifting for the H_d and H_a peaks for NIC is consistent with placement toward the water−AOT interface. The H_c peak initially shifted downfield and then slightly upfield, suggesting a placement near the water−AOT interface but more toward the AOT tails than H_d and H_a. The H_b peak was the only peak that consistently shifted upfield, suggesting the deepest placement (toward AOT tails) of all of the NIC protons. This data is consistent with NIC residing near the water−AOT interface with NIC tilted at the interface. This position would have H_a pointing toward the water pool and the amide tilted more toward the AOT headgroups. A similar finding was determined for the *ortho*-fluorobenzoate anion at the micellar interface.[53]

Finally, the placement and orientation of PIC within the RM samples were determined. The H_a doublet for PIC shifts slightly upfield from 8.63 ppm in the D_2O spectrum to 8.60 ppm in the w_0 8 spectrum. The peaks corresponding to H_b and H_c are overlapping in the D_2O spectrum but then separate within the RM samples with H_b shifting downfield gradually from 8.04 ppm in the D_2O spectrum to 8.24 ppm in the w_0 8 spectrum and H_c gradually shifting upfield from 8.02 ppm in the D_2O spectrum to 7.98 ppm in the w_0 8 spectrum. The H_d peak for PIC gradually shifts upfield from 7.64 ppm in the D_2O spectrum to 7.45 ppm in the w_0 8 spectrum. The upfield shifting pattern of H_a, H_c, and H_d peaks is consistent with the protons being placed toward the AOT tails. The downfield shifting pattern of H_b is consistent with it being placed more toward the AOT interface. This data is consistent with PIC residing near the AOT headgroups, with only H_b being near the AOT headgroups and the other protons toward the AOT tails causing a tilt of the molecule within the interface.

In summary, this data shows that these N-containing molecules interact differently with the AOT RM but reside at similar positions within the water−AOT interface. INH and iNIC were shown to reside within the AOT interface with the pyridine nitrogen facing toward the AOT tails and the hydrazide/amide toward the AOT headgroups. BHZ and BA were shown to reside deeper toward the AOT tails than INH or iNIC but with the same orientation. PIC was shown to reside at the AOT interface as INH and iNIC but slightly tilted at the interface with the nitrogen of the pyridine and the amide facing toward the AOT headgroup and water pool. NIC was also shown to be tilted with the proton between the amide and pyridine nitrogen facing the water pool. Generally, each molecule resided in similar positions, but the pyridine nitrogen to amide orientation did affected the overall molecular orientation at the water−AOT RM interface. This finding is similar to what has been shown for fluorobenzoate derivatives with micelles.[53]

^{1}H−^{1}H 2D NMR of Hydrazides and Amides within the AOT RM Interface. More information was sought to confirm the placement and orientation based on ^{1}H 1D NMR experiments; therefore, through-space ^{1}H−^{1}H 2D NOESY and ROESY experiments were conducted.[30,43−45] Both ^{1}H−^{1}H 2D NOESY and ROESY spectra with a 200 ms mixing time and higher concentration of BA were acquired to explore which experiment would provide the best signal-to-noise ratio (Figure S13). With the ROESY data producing a better signal-to noise ratio than NOESY for these samples, other ROESY spectra were sought using 100 or 0 ms mixing times. The 0 ms mixing time serves as a negative control to confirm no magnetization transfer was observed between magnetically different protons.

A portion of the ^{1}H−^{1}H 2D ROESY NMR spectra for INH and iNIC within w_0 12 RMs is shown in Figure 6. The spectra of INH within the w_0 12 RM microemulsion show a diagonal with two, negative, blue peaks corresponding to the H_a and H_b peaks of INH at 7.71 and 7.77 ppm, respectively. The positive, red, off-diagonal cross-peaks corresponding to H_a and H_b are observed in the spectra of 200 and 100 ms mixing time, whereas no cross-peaks are observed in the 0 ms mixing time spectrum as would be expected. In the 200 ms mixing time spectrum for INH, an off-diagonal cross-peak corresponding to H_b on INH and the methyl peak of either AOT or isooctane at 0.90 ppm on the f2 axis were observed. In the 100 ms mixing time spectrum, off-diagonal cross-peaks for both H_a and H_b at 0.90 ppm on the f2 axis were observed and correspond to the AOT or isooctane methyl peak. Considering that the previous ^{1}H 1D NMR experiments have shown that INH resides within the water−AOT interface, INH is most likely residing near the AOT ethyl CH_3 protons with the CH_3 protons tilted toward the interface (see Figure S12 for AOT assignments).

The spectra of the w_0 12 RM microemulsion with iNIC also indicated an interaction with the AOT interface similar to that for INH. Along the diagonal shown in Figure 6, two, negative, blue peaks corresponding to iNIC protons H_a and H_b at 8.70 and 7.80 ppm, respectively, are observed. Positive, red, off-diagonal cross-peaks between H_a and H_b in the 200 and 100 ms mixing time spectra are observed. Finally, no cross-peaks are observed in the 0 ms mixing time spectrum. In the 200 ms mixing time spectrum, positive, red, off-diagonal cross-peaks with H_a and H_b of iNIC are observed at 1.30 and 0.90 ppm on the f2 axis corresponding to the AOT CH_2 and an isooctane or AOT CH_3 peak, respectively. These peaks were not observed in either the 100 or 0 ms mixing time spectra. Because of iNIC's insolubility in isooctane and its similar placement determined by the ^{1}H 1D NMR studies, these results support the interpretation that iNIC interacts within the RM water−AOT resides at the interface near the sulfonate headgroups of the AOT similar to that in the vanadium dipicolinate complex.[54]

The ^{1}H−^{1}H 2D ROESY spectra of RMs containing BHZ and BA (Figure S14) were very similar. In the following, these compounds will be discussed concurrently. As can be seen on the diagonal of the spectra of BHZ, there are two negative, blue peaks at 7.97 and 7.43 ppm corresponding to H_a and H_b/H_c, respectively. Within the 200 and 100 ms mixing time spectra, positive, red, off-diagonal cross-peaks are observed between the H_a and H_b/H_c peaks, whereas no cross-peaks are observed for the 0 ms mixing time spectrum. In the 200 ms mixing time spectrum, positive, red, off-diagonal cross-peaks at 1.30 and 0.90 ppm on the f1 axis corresponding to the AOT CH_2, AOT CH_3, or isooctane CH_3 peak and H_a and H_b/H_c can be observed. In the spectrum using 100 ms mixing time, the same off-diagonal peaks are observed except for the off-diagonal cross-peak at 1.30 ppm on the f1 axis and 7.97 ppm on the f2 axis corresponding to the AOT CH_2 and the H_a protons, respectively. These cross-peaks were also observed for BA where the only differences in the spectra were from the placement of the BA negative, blue peaks on the diagonal at 7.92 ppm for H_a and 7.39 ppm for H_b/H_c. This data suggests

DOI: 10.1021/acs.langmuir.8b01661
Langmuir 2018, 34, 8939−8951

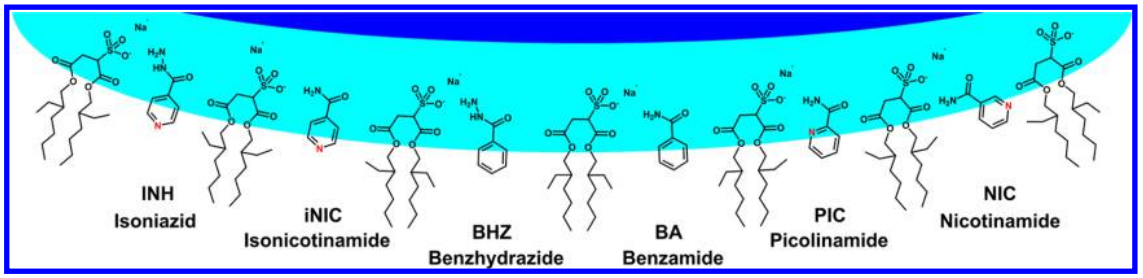

Figure 7. Pictorial representation of the placement of INH, iNIC, BHZ, BA, PIC, and NIC within the RM as determined through 1D and 2D ^{1}H NMR studies. It is important to note that this system is highly dynamic and therefore these are average positions/orientations within the AOT interface based on the 1D and 2D NMR data presented in this study.

that BHZ and BA are both positioned nearby the AOT ethyl with the hydrazide/amide facing the water pool consistent with the ^{1}H 1D NMR studies.

The ^{1}H−^{1}H 2D ROESY spectra of PIC, within RMs, were acquired to confirm the placement and orientation within the RM water−AOT interface. Figure S15 shows the ^{1}H−^{1}H 2D ROESY NMR spectra of PIC within the w_0 12 RM microemulsion acquired using 200, 100, and 0 ms mixing times. Observed in each of these spectra are negative, blue peaks along the diagonal corresponding to H_a (8.60 ppm), H_b (8.19 ppm), H_c (7.99 ppm), and H_d (7.47 ppm). In the spectra acquired using 200 and 100 ms mixing times, there are positive, red, off-diagonal cross-peaks between the peaks corresponding to the PIC peaks, whereas no off-diagonal cross-peaks are observed in the spectrum acquired using a 0 ms mixing time. In the 200 ms mixing time spectrum, positive, red, off-diagonal cross-peaks at 0.90 in the f1 dimension corresponding to all of the PIC peaks are observed. The same positive, red, off-diagonal cross-peaks are observed using a 100 ms mixing time with the exception of the off-diagonal cross-peak at 0.90 ppm in the f1 dimension and 7.99 ppm in the f2 dimension corresponding to H_c of PIC. This confirms that PIC resides within the AOT interface and does interact with the CH_3 of the ethyl of AOT.

The placement and orientation within RMs of NIC were explored using ^{1}H−^{1}H 2D ROESY NMR in the w_0 12 RM spectra shown in Figure S15. The peaks on the diagonal are negative, blue peaks corresponding to H_a (9.02 ppm), H_b (8.68 ppm), H_c (8.29 ppm), and H_d (7.50 ppm). Positive, red, off-diagonal cross-peaks between the NIC aromatic protons can be observed in the spectra acquired using 200 and 100 ms mixing times but not for the 0 ms mixing time spectrum. Positive, red, off-diagonal cross-peaks corresponding to AOT peaks can be observed at 0.90 ppm in the f1 dimension and at 9.02, 8.68, 8.29, and 7.50 ppm in the f2 dimension. These peaks suggest that all of the aromatic protons of NIC reside near a methyl. Three other positive, red, off-diagonal cross-peaks can be observed at 1.30 ppm in the f1 dimension and at 8.68, 8.29, and 7.50 ppm in the f2 dimension corresponding to the CH_2 AOT peak and H_b, H_c, and H_d. This data is consistent with NIC residing at the same position within the RM interface as the other probe molecules but H_a is not in proximity to the CH_2 of the AOT ethyl. By rotating the C−C bonds of the ethyl of AOT, the CH_3 of the ethyl can reach further than the CH_2, suggesting that H_a is in a position away from the CH_2. This would suggest a tilt in NIC at the water−AOT interface supporting the interpretation of the ^{1}H 1D NMR spectra.

In summary, the ^{1}H−^{1}H 2D ROESY NMR spectra of w_0 12 RMs containing the compounds of interest did support the results from the ^{1}H 1D NMR spectra. The placement of each of these molecules using data from both the 1D and 2D NMR experiments is illustrated in Figure 7. First of which, INH and iNIC both can be positioned near the AOT ethyl. Due to the similar ^{1}H 1D NMR chemical shifting patterns and similar ^{1}H-^{1}H 2D NMR experiments, they can be placed in similar positions near within the RM interface. BHZ and BA both can be placed at the same position and slightly deeper than iNIC and INH. The 2D NMR of PIC confirmed that it does reside within the interface of the water pool and AOT, whereas the 1D NMR suggested a tilt at the water−AOT interface. Briefly, all of the molecules resided near the water−AOT interface; however, PIC and NIC exhibited a tilted orientation within the interface (see Figure 7).

pK_a Measurement of the Hydrazides and Amides within the AOT RM. To explore how the AOT interface affects the aromatic N-containing molecules, the pK_a values of the small aromatic molecules were determined. The pH within the RM water pool is not just simply the $-\log[H^+]$ as is normally used in the United States to calculate pK_a in aqueous solutions.[55] The pH value within the RM water pool is much more complicated. Depending on the charge of the headgroup surfactant used to form the RM microemulsion, a proton gradient can form.[56,57] The AOT RMs used in this study have a negative charge and therefore can cause an increase in proton concentration at the interface.[47,55] The pK_a values of molecules have also been known to change within varying environments, such as the difference in pK_a values of a specific amino acid depends on whether or not it is in the center or on the surface of a protein; therefore, the RM may affect the small aromatic molecules' pK_a values.[58]

The pK_a values of the aromatic N-containing molecules in D_2O and in w_0 16 RMs are shown and compared to those in the literature and calculated values in Table 2.[59] The pK_a for BA was not determined in this study because of BA's low pK_a value. The pK_a values of each of the probe molecules in D_2O are all very similar to both the predicted pK_a values and the experimentally determined pK_a values.[59] The small differences between the pK_a values found in this study and the experimental studies in aqueous solutions is most likely caused by differences in ionic strength, temperature, and differences caused by H_2O (reported pK_a values) or D_2O (this study). Within the RMs, the pK_a of each molecule lowered beyond measurement. This would support an interaction with the AOT itself or an effect of the high ionic strength of the interface.[30,39,40,55] Either possibility supports that the molecules reside within the RM interface.

DLS of RMs Containing Aromatic Hydrazides and Amides. DLS was used to determine that RMs formed. In

DOI: 10.1021/acs.langmuir.8b01661
Langmuir 2018, 34, 8939−8951

Table 2. pK_a Values of the Hydrazides and Amides of Interest in Aqueous and RM Solutions[a]

compound	predicted pK_a	reported pK_a[59]	pK_a in D_2O	pK_a in w_0 16 RM
INH	3.4, 2.4*	3.5, 1.9*	3.3	<1
BHZ	2.8*	3.0*	2.8*	<1*
BA	−0.36	N.A.	N.A.	N.A.
PIC	2.2	2.1	2.4	<1
NIC	3.6	3.3	3.7	<1
iNIC	3.5	3.6	3.9	<1

[a]The table outlines the pK_a values determined using the method outlined in Figure S3. The pK_a values of the amine protons for INH and BZH are given by *. The predicted pK_a values are from http://www.chemicalize.org. The reported pK_a values are from ref 59.

addition to confirming that the RMs form, we also demonstrated that the sizes of the systems measured were consistent with those reported in the literature (Table S1).[41] Furthermore, the measurements were done to investigate whether the addition of the compound alters the overall structure of the RMs studied. As shown in Table S1, no differences in sizes of RMs with and without the aromatic hydrazides and aromatic amides were observed.[41]

Evaluation and Implication of Findings in Studies of Langmuir Monolayers and Interfaces in AOT−Isooctane RMs. Studies on model systems are done to obtain information that may not be accessible in studies of the biological membranes. The two model systems used in the studies here both have advantages and limitations. Regardless, it is important to note that there are substantial differences between the AOT interface and a phospholipid interface. The differences in structure, curvature, surfactant/lipid density, and headgroup charge (negative vs zwitterionic, respectively), may impact the interactions of the molecules under investigation with regard to their interaction with interfaces.[14,39,40,51] Although these differences exist, there are similarities between how the molecules of interest interact with the AOT interface and the phospholipid interface. By comparing the findings of the RM experiments with those of phospholipid Langmuir monolayer experiments, the combination can shed light on crucial differences behind the interactions of molecules with the surfactant or lipid interfaces.[30,45]

Interestingly, all of the molecules studied here were found to reside near the headgroup of the AOT surfactant interface. The RM studies provide information about how small structural changes in the aromatic amide or hydrazide can affect compound placement and orientation at a surfactant interface. This finding, albeit on a different type of interface, is consistent with the results reported in computational studies of NIC and PIC with phosphatidylcholine and phosphatidylethanolamine phospholipids[21,22] along with experimental studies with INH interacting with a liposome consisting of phosphotidylcholine.[60,61] We found that the distance of amide to the pyridine nitrogen and the molecular orientation of the amide can impact the interactions with the water−AOT interface. Similarly using computational methods in studies by Borba *et al.* and Martini *et al.*, specific hydrogen bondings with NIC and PIC were found using phosphatidylcholine and phosphatidylethanolamine phospholipids.[21,22] Although the findings in our studies with the RMs do not directly demonstrate the specific interactions with the phospholipid headgroups found in these computational studies, but the locations identified in our studies of the small aromatic N-containing molecules with the sulfonate headgroup of AOT were comparable, that is, placing the drug near the interface.

Conversely, if the small aromatic N-containing compounds interacted primarily with the phospholipid tails, then the headgroup would not have affected the overall interactions with the phospholipids and the area per phospholipid would have been affected similarly between DPPC and DPPE. Because this was shown to not be the case in the Langmuir monolayer studies, the molecules of interest most likely also reside near the phospholipid headgroups as found in the AOT RM experiments. The difference in interaction with DPPC versus DPPE was especially evident with INH and iNIC (see Figure 3A,B). The previous study by Marques *et al.* was able to determine a dissociation constant (K_d) of INH with dimyristoylphosphatidylcholine-supported bilayers to be 0.031 μmol by plasmon waveguide resonance.[60,62] With the observation that INH most likely prefers DPPE over DPPC, the K_d of INH with DPPE would be lower than that found by Marques *et al.* More studies are needed to determine the exact values and whether the difference in tail length would affect the K_d.

The Langmuir monolayer studies also support the interpretation that the orientation of the amide to pyridine nitrogen affects the phospholipid interface. This result was apparent from the differences in compression isotherm area per phospholipid caused by the presence of iNIC compared with NIC and PIC. NIC and PIC affected the monolayers similarly, in contrast to iNIC that affected the monolayers differently. iNIC was more similar to INH where it preferred DPPE, but iNIC did not spread the lipids like NIC and PIC did. The similar overall effects on the phospholipid monolayers by PIC and NIC were most likely caused by different molecular interactions that happen to have similar outcomes, as supported by a difference in tilting at the RM interface. To summarize, the specific structural characteristics of these compounds can influence their interactions with phospholipid and surfactant interfaces in a comparable manner.

When combining the information from these two model membrane systems, a few conclusions about the placement and interactions of the molecules of interest with surfactant and phospholipid interfaces can be made. The RM experiments show that despite a similar placement of all of the molecules of interest within the water−AOT interface, the orientation of the pyridine nitrogen to the amide can affect the specific orientation of the whole molecule of interest within an interface. This tilt of PIC and NIC suggests that within other interfaces, such as a phospholipid interface, the small difference between these molecules can allow for differences in the interactions with a phospholipid monolayer. However, these interactions will likely not be the same as those determined from the RM experiments.[21] The phospholipid Langmuir monolayer studies build on this idea by also supporting the expectation that the specifics behind the interactions of the headgroup of the phospholipid with the molecule of interest can affect binding such as what was observed with INH and iNIC. To summarize, the hypothesis that small differences in structure can lead to differences in the interactions of these small molecules with membrane interfaces was supported by these observations.

Although this study focused exclusively on monolayers, the observations gathered can cautiously be used to provide some

DOI: 10.1021/acs.langmuir.8b01661
Langmuir 2018, 34, 8939−8951

projections about how these molecules might pass through a bilayer membrane. With each molecule studied here, they all resided within the water−AOT RM interface and interacted differently with phospholipids containing the same tail but different headgroups. Together, these observations would support a headgroup-based interaction of the drugs in contrast to interactions with the choline, phosphate, or glycerol of phospholipids. Therefore, these compounds may not passively diffuse through a bilayer membrane-like weak acid preservatives (e.g., benzoic acid and formic acid) or protonophores (e.g., carbonyl cyanide *m*-chlorophenyl hydrazine).[8,10,30] If the molecules are able to traverse a membrane by passive diffusion, then it would be expected that the molecules would reside deeper within the RM tails/organic solvent.[30] The data obtained in this study does not support passive transport of these small aromatic N-containing compounds.

Other methods for crossing a bilayer have been extensively studied using different cations and anions. In these method, cations or anions are transported through forming a complex with phospholipids and then flip with the phospholipid across the bilayer or through a hydrophobic pore that may form allowing traversing of ions.[63−67] Some of these mechanisms have been studied through computational studies, and Borba *et al.* were able to show that the binding of PIC and NIC to the phosphatidylcholine or phosphatidylethanolamine headgroups can cause conformational differences in the phospholipid tails.[22] Considering that all of the molecules within this study interacted with the headgroups of AOT and the phospholipids, it is feasible that at least some of these molecules may affect the phospholipid tails as well. If these molecules affect the phospholipid tails, then such interaction might aid in the diffusion of the drugs across the phospholipid bilayer. Additional studies are needed to determine if these small molecules passively diffuse across bilayers, but these studies provide the framework to build a more in-depth understanding of small-molecule interactions with membrane interfaces.

CONCLUSIONS

We found that INH, BHZ, BA, PIC, NIC, and iNIC all interact with phospholipid and surfactant interfaces specficially with the phospholipid/surfactant headgroups but have different effects on phospholipid interfaces. The phospholipid Langmuir monolayer studies show a difference in interaction of the small molecules that were dependent on the structure of not only the small molecules but also the phospholipids themselves. All of the molecules tested reside within the water−AOT surfactant interface of RMs with the amide/hydrazide facing toward the water pool except for NIC and PIC. NIC and PIC resided at the interface but were tilted with the amide of NIC facing more away from the water pool than the amide of PIC. In summary, we show here that interactions of small aromatic N-containing molecules with lipid surfactant interfaces are not straightforward and that structural changes of the small aromatic compounds can alter their affinity for different phospholipid interfaces, how they affect different phospholipid interfaces, and the specifics behind the interactions with these interfaces.

ASSOCIATED CONTENT

Supporting Information

The Supporting Information is available free of charge on the ACS Publications website at DOI: 10.1021/acs.langmuir.8b01661.

Enlargement of Figures 1, 3, and 4; compression isotherm curves of DPPC and DPPE with DDI H_2O or 20 mM phosphate buffer (pH 7.4); the compression moduli graphs of DPPC and DPPE in the presence of the hydrazides and amides; an example for determination of the pK_a values using ^1H NMR; a table outlining the DLS results; a labeled AOT molecule for w_0 12 RM ^1H NMR spectrum; a comparison between $^1H-^1H$ 2D NMR NOESY and ROESY spectra of w_0 12 RMs containing BA; and $^1H-^1H$ 2D ROESY spectra obtained using varying mixing times of w_0 12 RMs containing BA, BHZ, PIC, and NIC (PDF)

AUTHOR INFORMATION

Corresponding Author

*E-mail: Debbie.crans@colostate.edu.

ORCID

Benjamin J. Peters: 0000-0002-6219-4897
Cameron Van Cleave: 0000-0002-0924-1738
Allison A. Haase: 0000-0001-6574-2599
Dean C. Crick: 0000-0001-9281-7058
Debbie C. Crans: 0000-0001-7792-3450

Author Contributions

The manuscript was written through contributions of all authors. All authors have given approval to the final version of the manuscript.

Notes

The authors declare no competing financial interest.

ACKNOWLEDGMENTS

We thank Dr. Christopher D. Rithner for assistance with the NMR studies. D.C.C. and D.C.C. thank NIH for funding for this research (Grant # AI119567) and the later by NSF (Grant # CHE-1709564).

ABBREVIATIONS

AOT, aerosol-OT; RM, reverse micelle; DPPC, dipalmitoylphosphatidylcholine; DPPE, dipalmitoylphosphatidylethanolamine; INH, isoniazid; BHZ, benzhydrazide; iNIC, isonicotinamide; NIC, nicotinamide; PIC, picolinamide; BA, benzamide; DLS, dynamic light scattering; NMR, nuclear magnetic resonance; R_h, hydrodynamic radius; DSS, 2,2-dimethyl-2-silapentane-5-sulfonate sodium salt; ROESY, rotating-frame Overhauser spectroscopy; NOESY, nuclear Overhauser effect spectroscopy; DDI H_2O, distilled deionized water

REFERENCES

(1) Azuma, K.; Ouchi, Y.; Inoue, S. Vitamin K: Novel Molecular Mechanisms of Action and Its Roles in Osteoporosis. *Geriatr. Gerontol. Int.* **2014**, *14*, 1−7.

(2) Lambert, R. J.; Stratford, M. Weak-Acid Preservatives: Modelling Microbial Inhibition and Response. *J. Appl. Microbiol.* **1999**, *86*, 157−164.

(3) Ullah, A.; Orij, R.; Brul, S.; Smits, G. J. Quantitative Analysis of the Modes of Growth Inhibition by Weak Organic Acids in *Saccharomyces cerevisiae*. *Appl. Environ. Microbiol.* **2012**, *78*, 8377−8387.

(4) Westfall, D. A.; Krishnamoorthy, G.; Wolloscheck, D.; Sarkar, R.; Zgurskaya, H. I.; Rybenkov, V. V. Bifurcation Kinetics of Drug Uptake by Gram-Negative Bacteria. *PLoS One* **2017**, *12*, No. e0184671.

(5) Zhang, Y.; Wade, M. M.; Scorpio, A.; Zhang, H.; Sun, Z. H. Mode of Action of Pyrazinamide: Disruption of *Mycobacterium*

DOI: 10.1021/acs.langmuir.8b01661
Langmuir 2018, 34, 8939−8951

tuberculosis Membrane Transport and Energetics by Pyrazinoic Acid. *J. Antimicrob. Chemother.* **2003**, *52*, 790−795.
(6) Bardou, F.; Raynaud, C.; Ramos, C.; Laneelle, M. A.; Laneelle, G. Mechanism of Isoniazid Uptake in *Mycobacterium tuberculosis*. *Microbiology* **1998**, *144*, 2539−2544.
(7) Unissa, A. N.; Subbian, S.; Hanna, L. E.; Selvakumar, N. Overview on Mechanisms of Isoniazid Action and Resistance in *Mycobacterium tuberculosis*. *Infect., Genet. Evol.* **2016**, *45*, 474−492.
(8) Finkelstein, A. Weak-Acid Uncouplers of Oxidative Phosphorylation - Mechanism of Action on Thin Lipid Membranes. *Biochim. Biophys. Acta, Bioenerg.* **1970**, *205*, 1−6.
(9) Olsson, A.; Olofsson, T.; Pero, R. W. Specific Binding and Uptake of Extracellular Nicotinamide in Human Leukemic K-562 Cells. *Biochem. Pharmacol.* **1993**, *45*, 1191−1200.
(10) Piper, P.; Mahe, Y.; Thompson, S.; Pandjaitan, R.; Holyoak, C.; Egner, R.; Muhlbauer, M.; Coote, P.; Kuchler, K. The Pdr12 Abc Transporter Is Required for the Development of Weak Organic Acid Resistance in Yeast. *EMBO J.* **1998**, *17*, 4257−4265.
(11) Silve, A.; Mir, L. M. Cell Electropermeabilization and Cellular Uptake of Small Molecules: The Electrochemotherapy Concept. *Clin. Asp. Electroporation* **2011**, 69−82.
(12) Wilson, D. F.; Ting, H. P.; Koppelman, M. S. Mechanism of Action of Uncouplers of Oxidative Phosphorylation. *Biochemistry.* **1971**, *10*, 2897−2902.
(13) Ivanova, N.; Ivanova, A. Testing the Limits of Model Membrane Simulations-bilayer Composition and Pressure Scaling. *J. Comput. Chem.* **2018**, *39*, 387−396.
(14) Singer, S. J.; Nicolson, G. L. The Fluid Mosaic Model of the Structure of Cell Membranes. *Science* **1972**, *175*, 720−730.
(15) van Meer, G.; Voelker, D. R.; Feigenson, G. W. Membrane Lipids: Where They Are and How They Behave. *Nat. Rev. Mol. Cell Biol.* **2008**, *9*, 112−124.
(16) Álvarez, R.; Aramburu, L.; Puebla, P.; Caballero, E.; González, M.; Vicente, A.; Medarde, M.; Peláez, R. Pyridine Based Antitumour Compounds Acting at the Colchicine Site. *Curr. Med. Chem.* **2016**, *23*, 1100−1130.
(17) Nayyar, A.; Jain, R. Recent Advances in New Structural Classes of Anti-Tuberculosis Agents. *Curr. Med. Chem.* **2005**, *12*, 1873−1886.
(18) Prachayasittikul, S.; Pingaew, R.; Worachartcheewan, A.; Sinthupoom, N.; Prachayasittikul, V.; Ruchirawat, S.; Prachayasittikul, V. Roles of Pyridine and Pyrimidine Derivatives as Privileged Scaffolds in Anticancer Agents. *Mini-Rev. Med. Chem.* **2017**, *17*, 869−901.
(19) Borba, A.; Albrecht, M.; Gomez-Zavaglia, A.; Lapinski, L.; Nowak, M. J.; Suhm, M. A.; Fausto, R. Dimer Formation in Nicotinamide and Picolinamide in the Gas and Condensed Phases Probed by Infrared Spectroscopy. *Phys. Chem. Chem. Phys.* **2008**, *10*, 7010−7021.
(20) Borba, A.; Gomez-Zavaglia, A.; Fausto, R. Molecular Structure, Vibrational Spectra, Quantum Chemical Calculations and Photochemistry of Picolinamide and Isonicotinamide Isolated in Cryogenic Inert Matrixes and in the Neat Low-Temperature Solid Phases. *J. Phys. Chem. A* **2008**, *112*, 45−57.
(21) Martini, M. F.; Disalvo, E. A.; Pickholz, M. Nicotinamide and Picolinamide in Phospholipid Monolayers. *Int. J. Quantum Chem.* **2012**, *112*, 3289−3295.
(22) Borba, A.; Lairion, F.; Disalvo, A.; Fausto, R. Interaction of Nicotinamide and Picolinamide with Phosphatidylcholine and Phosphatidylethanolamine Membranes: A Combined Approach Using Dipole Potential Measurements and Quantum Chemical Calculations. *Biochim. Biophys. Acta, Biomembr.* **2009**, *1788*, 2553−2562.
(23) Gzyl-Malcher, B.; Handzlik, J.; Nowak-Stępniowska, A. Interactions of Phenytoin with Lipids in Mixed Langmuir Monolayers. *Colloids Surf., A* **2008**, *321*, 52−59.
(24) Gzyl-Malcher, B.; Handzlik, J.; Klekowska, E. Interaction of Prazosin with Model Membranes - a Langmuir Monolayer Study. *Bioelectrochemistry* **2012**, *87*, 96−103.
(25) Jurak, M. Thermodynamic Aspects of Cholesterol Effect on Properties of Phospholipid Monolayers: Langmuir and Langmuir-Blodgett Monolayer Study. *J. Phys. Chem. B* **2013**, *117*, 3496−3502.
(26) Hoyo, J.; Torrent-Burgues, J.; Guaus, E. Biomimetic Monolayer Films of Monogalactosyldiacylglycerol Incorporating Ubiquinone. *J. Colloid Interface Sci.* **2012**, *384*, 189−197.
(27) Nerdal, W.; Nilsen, T. R. S.; Steinkopf, S. Coenzyme Q(10), Localizations in Model Membranes. A Langmuir Monolayer Study. *Biophys. Chem.* **2015**, *207*, 74−81.
(28) Roche, Y.; Peretti, P.; Bernard, S. Influence of the Chain Length of Ubiquinones on Their Interaction with DPPC in Mixed Monolayers. *Biochim. Biophys. Acta, Biomembr.* **2006**, *1758*, 468−478.
(29) Choi, Y.; Attwood, S. J.; Hoopes, M. I.; Drolle, E.; Karttunen, M.; Leonenko, Z. Melatonin Directly Interacts with Cholesterol and Alleviates Cholesterol Effects in Dipalmitoylphosphatidylcholine Monolayers. *Soft Matter.* **2014**, *10*, 206−213.
(30) Peters, B. J.; Groninger, A. S.; Fontes, F. L.; Crick, D. C.; Crans, D. C. Differences in Interactions of Benzoic Acid and Benzoate with Interfaces. *Langmuir* **2016**, *32*, 9451−9459.
(31) Sostarecz, A. G.; Gaidamauskas, E.; Distin, S.; Bonetti, S. J.; Levinger, N. E.; Crans, D. C. Correlation of Insulin-Enhancing Properties of Vanadium-Dipicolinate Complexes in Model Membrane Systems: Phospholipid Langmuir Monolayers and AOT Reverse Micelles. *Chem. − Eur. J.* **2014**, *20*, 5149−5159.
(32) Chimote, G.; Banerjee, R. Effect of Antitubercular Drugs on Dipalmitoylphosphatidylcholine Monolayers: Implications for Drug Loaded Surfactants. *Respir. Physiol. Neurobiol.* **2005**, *145*, 65−77.
(33) Kaganer, V. M.; Mohwald, H.; Dutta, P. Structure and Phase Transitions in Langmuir Monolayers. *Rev. Mod. Phys.* **1999**, *71*, 779−819.
(34) Veldhuizen, E. J. A.; Haagsman, H. P. Role of Pulmonary Surfactant Components in Surface Film Formation and Dynamics. *Biochim. Biophys. Acta, Biomembr.* **2000**, *1467*, 255−270.
(35) Veldhuizen, R.; Nag, K.; Orgeig, S.; Possmayer, F. The Role of Lipids in Pulmonary Surfactant. *Biochim. Biophys. Acta, Mol. Basis Dis.* **1998**, *1408*, 90−108.
(36) Wüstneck, R.; Perez-Gil, J.; Wüstneck, N.; Cruz, A.; Fainerman, V. B.; Pison, U. Interfacial Properties of Pulmonary Surfactant Layers. *Adv. Colloid Interface Sci.* **2005**, *117*, 33−58.
(37) Nowotarska, S. W.; Nowotarski, K. J.; Friedman, M.; Situ, C. Effect of Structure on the Interactions between Five Natural Antimicrobial Compounds and Phospholipids of Bacterial Cell Membrane on Model Monolayers. *Molecules* **2014**, *19*, 7497−7515.
(38) Sohlenkamp, C.; Geiger, O. Bacterial Membrane Lipids: Diversity in Structures and Pathways. *FEMS Microbiol. Rev.* **2016**, *40*, 133−159.
(39) De, T. K.; Maitra, A. Solution Behavior of Aerosol Ot in Nonpolar-Solvents. *Adv. Colloid Interface Sci.* **1995**, *59*, 95−193.
(40) Eicke, H. F.; Rehak, J. Formation of Water-Oil-Microemulsions. *Helv. Chim. Acta* **1976**, *59*, 2883−2891.
(41) Maitra, A. Determination of Size Parameters of Water Aerosol OT Oil Reverse Micelles from Their Nuclear Magnetic-Resonance Data. *J. Phys. Chem.* **1984**, *88*, 5122−5125.
(42) Zulauf, M.; Eicke, H. F. Inverted Micelles and Microemulsions in the Ternary-System H2o-Aerosol-Ot-Isooctane as Studied by Photon Correlation Spectroscopy. *J. Phys. Chem.* **1979**, *83*, 480−486.
(43) Crans, D. C.; Trujillo, A. M.; Bonetti, S.; Rithner, C. D.; Baruah, B.; Levinger, N. E. Penetration of Negatively Charged Lipid Interfaces by the Doubly Deprotonated Dipicolinate. *J. Org. Chem.* **2008**, *73*, 9633−9640.
(44) Crans, D. C.; Trujillo, A. M.; Pharazyn, P. S.; Cohen, M. D. How Environment Affects Drug Activity: Localization, Compartmentalization and Reactions of a Vanadium Insulin-Enhancing Compound, Dipicolinatooxovanadium(V). *Coord. Chem. Rev.* **2011**, *255*, 2178−2192.
(45) Koehn, J. T.; Magallanes, E. S.; Peters, B. J.; Beuning, C. N.; Haase, A. A.; Zhu, M. J.; Rithner, C. D.; Crick, D. C.; Crans, D. C. A Synthetic Isoprenoid Lipoquinone, Menaquinone-2, Adopts a Folded

DOI: 10.1021/acs.langmuir.8b01661
Langmuir 2018, 34, 8939−8951

Conformation in Solution and at a Model Membrane Interface. *J. Org. Chem.* **2018**, *83*, 275−288.
(46) Samart, N.; Beuning, C. N.; Haller, K. J.; Rithner, C. D.; Crans, D. C. Interaction of a Biguanide Compound with Membrane Model Interface Systems: Probing the Properties of Antimalaria and Antidiabetic Compounds. *Langmuir* **2014**, *30*, 8697−8706.
(47) Sripradite, J.; Miller, S.; Tongraar, A.; Johnson, M.; Crans, D. How Interfaces Affect the Acidity of the Anilinium Ion. *Chem. - Eur. J.* **2016**, *22*, 3873−3880.
(48) Leekumjorn, S.; Sum, A. K. Molecular Simulation Study of Structural and Dynamic Properties of Mixed DPPC/DPPE Bilayers. *Biophys. J.* **2006**, *90*, 3951−3965.
(49) Leekumjorn, S.; Sum, A. K. Molecular Investigation of the Interactions of Trehalose with Lipid Bilayers of DPPC, DPPE and Their Mixture. *Mol. Simul.* **2006**, *32*, 219−230.
(50) Wang, Z.; Yang, S. Effects of Fullerenes on Phospholipid Membranes: A Langmuir Monolayer Study. *ChemPhysChem* **2009**, *10*, 2284−2289.
(51) Jones, M. N. *Micelles, Monolayers, and Biomembranes*; Wiley-Liss: New York, 1995.
(52) Crans, D. C.; Peters, B. J.; Wu, X.; McLauchlan, C. C. Does Anion-Cation Organization in Na^+-Containing X-Ray Crystal Structures Relate to Solution Interactions in Inhomogeneous Nanoscale Environments: Sodium-Decavanadate in Solid State Materials, Minerals, and Microemulsions. *Coord. Chem. Rev.* **2017**, *344*, 115−130.
(53) Vermathen, M.; Stiles, P.; Bachofer, S. J.; Simonis, U. Investigations of Monofluoro-Substituted Benzoates at the Tetradecyltrimethylammonium Micellar Interface. *Langmuir* **2002**, *18*, 1030−1042.
(54) Crans, D. C.; Rithner, C. D.; Baruah, B.; Gourley, B. L.; Levinger, N. E. Molecular Probe Location in Reverse Micelles Determined by NMR Dipolar Interactions. *J. Am. Chem. Soc.* **2006**, *128*, 4437−4445.
(55) Crans, D. C.; Levinger, N. E. The Conundrum of Ph in Water Nanodroplets: Sensing Ph in Reverse Micelle Water Pools. *Acc. Chem. Res.* **2012**, *45*, 1637−1645.
(56) Baruah, B.; Roden, J. M.; Sedgwick, M.; Correa, N. M.; Crans, D. C.; Levinger, N. E. When Is Water Not Water? Exploring Water Confined in Large Reverse Micelles Using a Highly Charged Inorganic Molecular Probe. *J. Am. Chem. Soc.* **2006**, *128*, 12758−12765.
(57) Majumder, R.; Sarkar, Y.; Das, S.; Ray, A.; Parui, P. P. Interfacial Ph and Polarity Detection of Amphiphilic Self-Assemblies Using a Single Schiff-Base Molecule. *New J. Chem.* **2017**, *41*, 8536−8545.
(58) Moran, L.; Scrimgeour, K.; Horton, H.; Ochs, R.; Rawn, J. *Biochemistry*, 2nd ed.; Neil Patterson, 1994.
(59) Perrin, D. D. International Union of Pure and Applied Chemistry, Analytical Chemistry Division, Commission on Electroanalytical Chemistry. *Dissociation Constants of Organic Bases in Aqueous Solution*; Butterworths: London, 1965.
(60) Marques, A. V.; Trindade, P. M.; Marques, S.; Brum, T.; Harte, E.; Rodrigues, M. O.; D'Oca, M. G. M.; da Silva, P. A.; Pohlmann, A. R.; Alves, I. D.; de Lima, V. R. Isoniazid Interaction with Phosphatidylcholine-Based Membranes. *J. Mol. Struct.* **2013**, *1051*, 237−243.
(61) Rodrigues, C.; Gameiro, P.; Prieto, M.; de Castro, B. Interaction of Rifampicin and Isoniazid with Large Unilamellar Liposomes: Spectroscopic Location Studies. *Biochim. Biophys. Acta, Gen. Subj.* **2003**, *1620*, 151−159.
(62) Tollin, G.; Salamon, Z.; Hruby, V. J. Techniques: Plasmon-Waveguide Resonance (PWR) Spectroscopy as a Tool to Study Ligand-Gpcr Interactions. *Trends Pharmacol. Sci.* **2003**, *24*, 655−659.
(63) Contreras, F. X.; Sánchez-Magraner, L.; Alonso, A.; Goñi, F. M. Transbilayer (Flip-Flop) Lipid Motion and Lipid Scrambling in Membranes. *FEBS Lett.* **2010**, *584*, 1779−1786.
(64) Gurtovenko, A. A.; Vattulainen, I. Molecular Mechanism for Lipid Flip-Flops. *J. Phys. Chem. B* **2007**, *111*, 13554−13559.
(65) Henseleit, U.; Plasa, G.; Haest, C. Effects of Divalent-Cations on Lipid Flip-Flop in the Human Erythrocyte-Membrane. *Biochim. Biophys. Acta, Biomembr.* **1990**, *1029*, 127−135.
(66) Kandasamy, S. K.; Larson, R. G. Cation and Anion Transport through Hydrophilic Pores in Lipid Bilayers. *J. Chem. Phys.* **2006**, *125*, No. 07491.
(67) Smeets, E. F.; Comfurius, P.; Bevers, E. M.; Zwaal, R. F. A. Calcium-Induced Transbilayer Scrambling of Fluorescent Phospholipid Analogs in Platelets and Erythrocytes. *Biochim. Biophys. Acta, Biomembr.* **1994**, *1195*, 281−286.

DOI: 10.1021/acs.langmuir.8b01661
Langmuir 2018, 34, 8939−8951